Proceedings of OMAE 2004
23rd International Conference on Offshore Mechanics and Arctic Engineering
20-25 June 2004 Vancouver

OMAE2004-51084

WAVE RUN UP AS IMPORTANT HYDRODYNAMIC ISSUE FOR GRAVITY BASED STRUCTURES

Erwin Loots

MARIN
PO Box 28
6700 AA Wageningen
The Netherlands

Bas Buchner

MARIN
PO Box 28
6700 AA Wageningen
The Netherlands

ABSTRACT

Gravity Based Structures (GBS) are now seriously considered as LNG import terminal. When the environment of wind and waves is strongly directional, with an optimum orientation of the GBS a significant shielding can be achieved, reducing the weather downtime. However, the application of Gravity Based Structures also results in a number of hydrodynamic challenges, of which wave run-up is the subject of the present paper.

Because of the optimized heading of the GBS beam to the dominant sea direction, typically the survival conditions will be beam to the GBS as well. This means that the wave run-up and possible green water on the deck of the GBS is a problem that needs serious evaluation.

This run up problem is studied numerically with an improved Volume Of Fluid (iVOF) method. Results are presented concerning the generation and propagation of waves, the influence of deflectors, and the effect of wind.

INTRODUCTION

Recently, several companies have begun investigating the possibility of building a Gravity Based Structure (GBS) as an offshore terminal for the importation of liquefied natural gas. The structures are likely to be rectangular caissons which will serve as breakwaters for the LNG tankers. They will also store the LNG and support the re-gasification equipment. There are considerable challenges in the analysis of wave interaction with this type of structure, see also Buchner, Loots, Forristal and Van Iperen (2004).

Because of the optimized heading of the GBS beam to the dominant sea direction, typically the survival conditions will be beam to the GBS as well. This means that the wave run-up and possible green water on the deck of the GBS is a problem that needs serious evaluation. Numerical simulations with an improved Volume Of Fluid (iVOF) method called ComFLOW were used to predict the wave run up against a LNG GBS.

Figure 1: Gravity Based Structure as LNG import terminal

The rest of this paper consists of a short description of observation model tests, and then the basic features of the numerical model are explained. After that, wave generation and propagation is discussed. The simulations focus on the problem of the handling of the run-up in front of the GBS. The effect of a deflector and the influence of wind are investigated.

OBSERVATION TESTS ON WAVE RUN-UP

A limited series of visual model tests were carried out to study the main physics of the run up. Because the depth does not exceed 17 m, wave heights were limited to approximately 10 m; higher waves break down rapidly. The most important observation is the strong non-linear run up in front of the GBS, resulting in a water jet shooting up high into the air, far above the GBS deck (see Figure 2 and Figure 3).

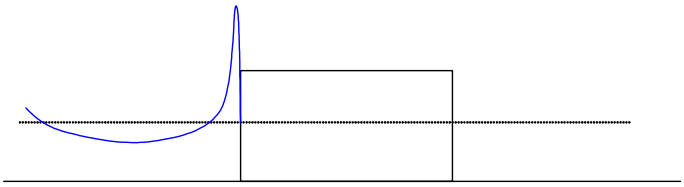

Figure 2 : Typical run up in front of a GBS

.

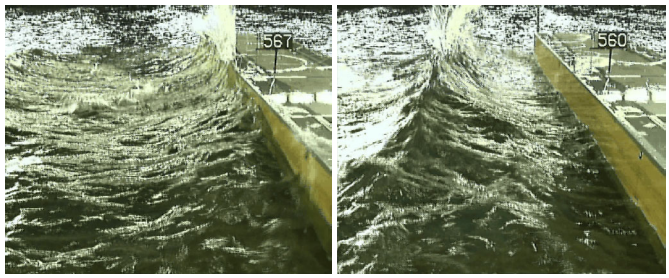

Figure 3: Wave run up at the GBS (left) and 'fountain'-type breaking at some distance from the GBS (right)

It is very important to note that there exists a strong non-linear interaction between the waves reflected at the GBS and the incoming waves, see Figure 3 and Figure 4.

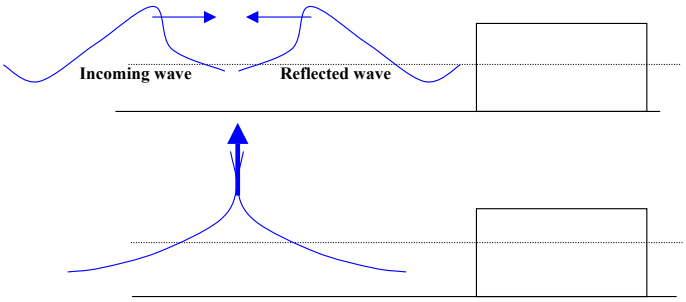

Figure 4: **Strong non-linear interaction between the waves reflected at the GBS and the incoming waves, resulting in 'fountain'-type wave breaking**

Because the waves are steep and close to breaking, their horizontal crest velocities are high. When they meet each other in opposite directions, 'fountain'-type wave breaking occur at some distance from the GBS. This type of effects influence the incoming wave, and consequently the wave run up, significantly. This influence should be taken into account in run up tests and simulations. The run up of the largest wave in a realistic wave group will be affected by the previous (lower) waves in the group that have reflected on the structure already. Single event tests and simulations are consequently not sufficient.

In the remainder of this paper, we will focus on numerical simulations.

DESCRIPTION OF THE NUMERICAL SIMULATION METHOD

ComFLOW is an improved 3D Volume Of Fluid (iVOF) Navier-Stokes solver. The program has been developed initially by the University of Groningen/RuG (Prof.dr. Arthur Veldman) to study the sloshing of liquid fuel in satellites. This micro-gravity environment requires a very accurate and robust description of the free surface. Coupled dynamics between the sloshing fluid and the satellite were investigated as well (Gerrits, 1999 and 2001). In close co-operation with MARIN, this methodology was later extended to the calculation of green water loading on a fixed bow deck (Fekken, 1999; Buchner, 2001), see Figure 5. Also anti-roll tanks, including the coupling with ship motions (van Daalen, 2000), were investigated. Furthermore, the entry of a wedge in a fluid was studied as part of the RuG-MARIN co-operation, as well as the wave impact loads on fixed structures (Kleefsman 2002; Figure 6).

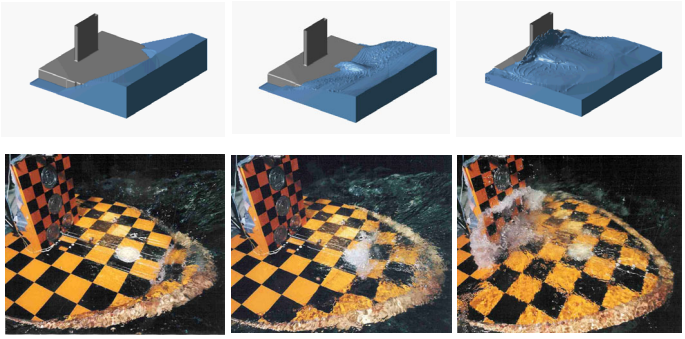

Figure 5: Example of earlier application of the method: green water on the deck of an FPSO

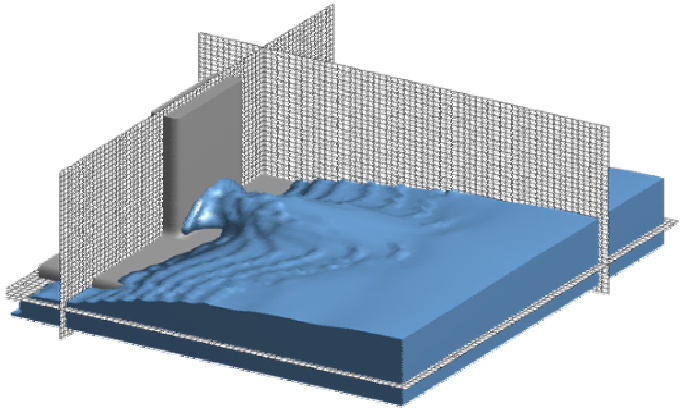

Figure 6: Wave impact simulation; 3D grid also shown

The Volume Of Fluid (VOF) algorithm as developed by Hirt and Nichols (1981) is used as a basis for the fluid advection. The method solves the incompressible Navier-Stokes equations with a free-surface condition on the free boundary. In the VOF method a VOF function F (with values between 0 and 1) is used, indicating which part of the cell is filled with fluid. The VOF method reconstructs the free surface in each computational cell. This makes it suitable for the prediction of all phases of the local free surface problem.

First the mathematical and numerical model will be summarised. This will be limited to the main aspects, because the detailed numerical aspects are outside the scope of the present paper. Excellent overviews of the numerical details of the method can be found in the references mentioned above. To distinguish between the original VOF method of Hirt and Nichols (1981) and the present method with its extensive number of modifications, the name improved-VOF (iVOF) method will be used in the rest of this paper.

Mathematical model

The incompressible Navier-Stokes equations describe the motions of a fluid in general terms. They are based on conservation of mass (Expression 1) and momentum (Expressions 2 through 4).

$$\frac{\partial u}{\partial x}+\frac{\partial v}{\partial y}+\frac{\partial w}{\partial z}=0 \tag{1}$$

$$\frac{\partial u}{\partial t}+u\frac{\partial u}{\partial x}+v\frac{\partial u}{\partial y}+w\frac{\partial u}{\partial z}=-\frac{1}{\rho}\frac{\partial p}{\partial x}+\nu\left(\frac{\partial^2 u}{\partial x^2}+\frac{\partial^2 u}{\partial y^2}+\frac{\partial^2 u}{\partial z^2}\right)+F_x \tag{2}$$

$$\frac{\partial v}{\partial t}+u\frac{\partial v}{\partial x}+v\frac{\partial v}{\partial y}+w\frac{\partial v}{\partial z}=-\frac{1}{\rho}\frac{\partial p}{\partial y}+\nu\left(\frac{\partial^2 v}{\partial x^2}+\frac{\partial^2 v}{\partial y^2}+\frac{\partial^2 v}{\partial z^2}\right)+F_y \tag{3}$$

$$\frac{\partial w}{\partial t}+u\frac{\partial w}{\partial x}+v\frac{\partial w}{\partial y}+w\frac{\partial w}{\partial z}=-\frac{1}{\rho}\frac{\partial p}{\partial z}+\nu\left(\frac{\partial^2 z}{\partial x^2}+\frac{\partial^2 z}{\partial y^2}+\frac{\partial^2 z}{\partial z^2}\right)+F_z \tag{4}$$

With:

p	=	pressure
t	=	time
u	=	velocity in x-direction
v	=	velocity in y-direction
w	=	velocity in z-direction
x	=	x-position
y	=	y-position
z	=	z-position
ν	=	kinematic viscosity
ρ	=	fluid density

$\vec{F}=(F_x, F_y, F_z)$ is an external body force, such as gravity. $\vec{F}$ can also contain virtual body forces: instead of actually moving the solid body in the numerical model, the fluid can be subjected to an acceleration (equal in magnitude but opposite in sign) to account for solid-body motion.

The Navier-Stokes equations can also be written in a shorter notation as:

$$\nabla\cdot\vec{u}=0 \tag{5}$$

$$\frac{\partial\vec{u}}{\partial t}+\nabla p=\vec{R} \tag{6}$$

$\vec{R}$ now contains all convective, diffusive and body forces.

Numerical model: geometry and free surface description

For the discretisation of a computational domain in numerical simulations a large number of different methods are available. Basically, they can be divided into:

- Structured and unstructured grids
- Boundary fitted and non-boundary fitted grids

In the improved-VOF method a structured (Cartesian) non-boundary fitted grid (not necessarily equidistant) is chosen. This has the following advantages related to the use of the method for the prediction of wave loading:

- Easy generation of the grid around complex structures
- A lot of research on surface tracking on orthogonal grids has been carried out
- Moving objects in the fluid can be dealt with in a similar way as fixed boundaries, without re-gridding

The main disadvantage of this discretisation method is the fact that the boundary and free surface are generally not aligned with the gridlines. This requires special attention in the solution method, as will be shown below.

An indicator function is used in the form of volume and edge apertures to track the amount of flow in a cell and through a cell face:

- Volume aperture: the geometry aperture F_b indicates which fraction of a cell is allowed to contain fluid ($0 \le F_b \le 1$). For bodies moving through the fluid, the geometry aperture may vary in time. The time-dependent fluid aperture F_s indicates which fraction of a cell is actually occupied by fluid and satisfies the relation $0 \le F_s \le F_b$.
- Edge aperture: the edge apertures A_x, A_y, and A_z define the fraction of a cell surface through which fluid may flow in the x, y and z direction respectively. Obviously, these apertures are between zero and one.

Figure 7 shows a two-dimensional example with $F_b = 0.8$ and $F_s = 0.3$.

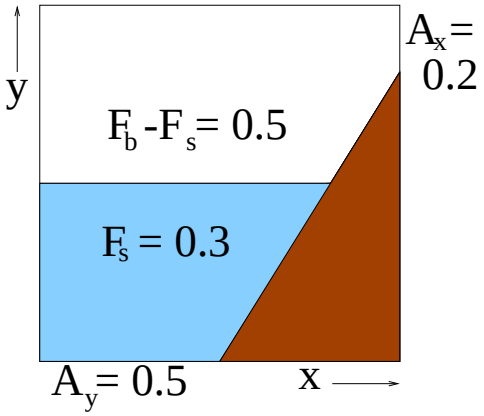

Figure 7: Two-dimensional example of a grid cell using apertures

After the apertures have been assigned to the grid cells and the cell edges, every cell is given a label to distinguish between boundary, air and fluid. Two classes of labelling exist: Geometry cell labels and fluid cell labels. The geometry labelling at each time step divides the cells into three classes:

F(low)-cells : All cells with $F_b \geq 0$

B(oundary)-cells : All cells adjacent to a **F**-cell

(e)**X**(ternal)-cells : All remaining cells

The free-surface cell labelling is a subdivision of the **F**-cells. The subdivision consists of 3 subclasses:

E(mpty) cells : All cells with $F_s = 0$

S(urface) cells : All cells adjacent to an **E**-cell

F'(luid)-cells : All remaining **F**-cells

Figure 8 shows an example of geometry cell labelling and free-surface cell labelling for a wedge entering a fluid.

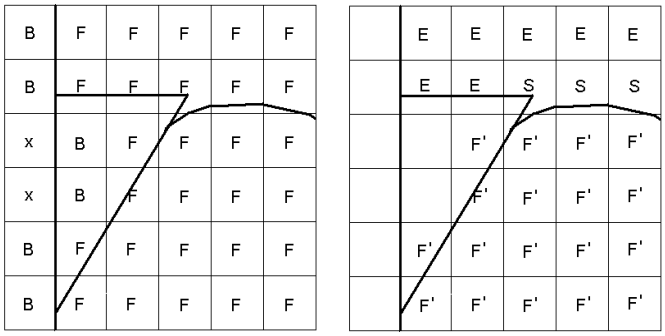

Figure 8: Geometry cell labelling (left) and free-surface cell label for a wedge entering a fluid (right)

The discretisation of the Navier-Stokes equations is done on a staggered grid, which means that the pressure will be set in the cell centres and the velocity components in the middle of the cell faces between two cells. This is shown in 2D in Figure 9.

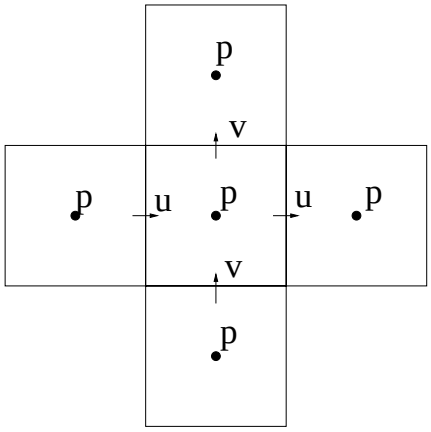

Figure 9: Location of the pressure and velocity components in the staggered grid

The Navier-Stokes equations, as given by Eqns. (5) and (6), are discretised in time according to the explicit first order Forward Euler method as follows:

$$\nabla.\vec{u}^{n+1} = 0 \tag{7}$$

$$\frac{\vec{u}^{n+1} - \vec{u}^{n}}{\Delta t} + \nabla p^{n+1} = \vec{R}^{n} \tag{8}$$

Δt is the time step and n+1 and n denote the new and old time level, respectively. The conservation of mass in Expression (7) and the pressure in Expression (8) are treated on the new time level n+1 to assure that the new $\vec{u}$ is divergence-free (no gain or loss of fluid). The choice for an explicit first-order method is justified by the fact that the fluid has to be advected properly each time step. All involved coefficient matrices are therefore time-dependent.

The spatial discretisation will now be explained using the computational cell shown in Figure 10.

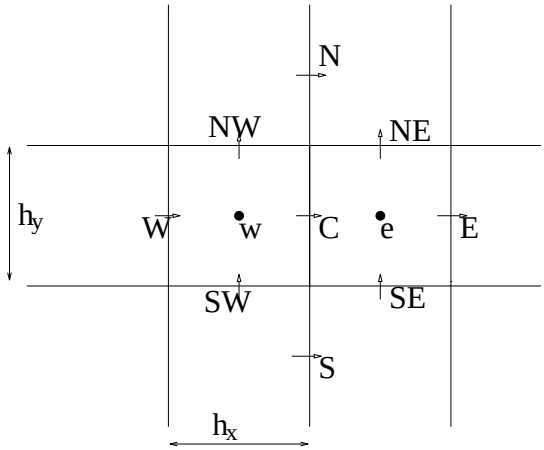

Figure 10: Spatial discretisation cell, using compass indication for cell phases

Expression (7) is applied in the centres of the cells and a central discretisation is used. In the cell with centre w the discretised equation becomes:

$$\frac{u_C^{n+1} - u_W^{n+1}}{h_x} + \frac{v_{NW}^{n+1} - v_{SW}^{n+1}}{h_y} = 0 \qquad (9)$$

The momentum Expression (8) is applied in the centres of the cell faces, thus the discretisation in point C becomes:

$$\frac{u_C^{n+1} - u_C^n}{\Delta t} + \frac{p_e^{n+1} - p_w^{n+1}}{h_x} = R_C^n \qquad (10)$$

In the detailed work of Gerrits (2001) other aspects of the numerical method are described in detail, such as:

- Discretisation of R_c^n
- Discretisation near the free-surface
- In- and outflow discretisation
- Pressure Poisson equation
- Free surface reconstruction and displacement
- Use of the Courant-Friedrichs-Levy (CFL) number
- Calculation of forces

The following functionalities are presently available in ComFLOW :

- Calculation of the fluid motion by solving the incompressible Navier-Stokes equations.
- One type of fluid flow is considered, with a void where no fluid is present.
- Possibility to model an arbitrary number of fixed objects in the fluid. The objects are defined piecewise linearly.
- Options to use no-slip or free-slip boundary conditions at the solid boundaries. At the free surface continuity of tangential and normal stresses (including capillary effects) is prescribed. Inflow and outflow boundary conditions for fluid velocities and/or pressures can be defined.
- The fluid simulations are carried out on a Cartesian grid with user-defined stretching. The Cartesian grid is fixed in the domain. When the domain is moving a virtual body force is added to the forcing term in the Navier-Stokes equations. The fluid motions are thus solved in a domain-fixed co-ordinate system.
- To distinguish between the different characters of grid cells, the cells are labelled. The Navier-Stokes equations are discretised and solved in cells that contain fluid. The free-surface displacement is described by the Volume Of Fluid method with a local height function.
- The generation of waves, which has been accomplished by specifying fluid velocities at the inflow boundary of the fluid domain? The fluid velocities are obtained from potential flow. Linear waves (Airy waves) and fifth-order waves (Stokes waves) have been implemented. The linear waves have been stretched towards the actual position of the free surface using Wheeler stretching.
- Several absorbing boundary conditions at the outflow boundaries.
- The possibility to use the velocity field from a (de-coupled) linear diffraction theory. Linear diffraction theory is used to compute body motions and fluid velocities which are then used in ComFLOW to prescribe the body motions and fluid velocities on the inflow and outflow boundaries.
- An off-line coupling with a structural-analysis code has been established to compute the response of a structure to high peak loads.

APPLICATION OF THE IVOF METHOD TO THE GBS WAVE RUN UP PROBLEM

The general idea is to create a wave, using a numerical wave maker on the left-hand side of the (2D) computational domain, which reaches a maximum height at a predefined focus point (a so-called NewWave). At this point the GBS structure will be placed, see Figure 11. As observed in the basin tests, the waves are breaking or close to breaking in shallow water. Therefore, it was decided to generate the waves in relatively deep water: 30 m instead of the prescribed 17m. Then the generated waves run onto a slope. At the end of the slope the water depth has the desired value while the waves at that point are still regular.

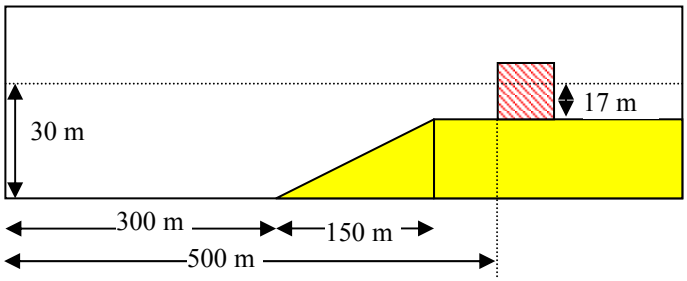

Figure 11: Computational domain

Generation of waves

First the NewWave theory (Tromans, 1991) was used to generate waves according to the specified parameters. In principle, the NewWave is completely described by the four vectors

$$A(i), \kappa(i), \omega(i), \varphi(i)$$

(denoting respectively the amplitude, wave number, angular frequency and phase shift) which form the wave according to

$$\eta(x,t) = \sum_{i=1}^{N} A(i)\cos(\kappa(i)x - \omega(i)t + \varphi(i)),$$

This expression will reach a maximum at a certain x (the focus point) and corresponding time T_s.

These vectors were read by the ComFLOW code and at the left-hand side of the domain this summation of linear waves can be generated by the wave maker. Thus, at each time step, the numerical wave generator sets the water height and corresponding velocities, using Wheeler stretching near the free surface. Plots of the theoretical wave, both temporal and spatial, are shown in Figure 12.

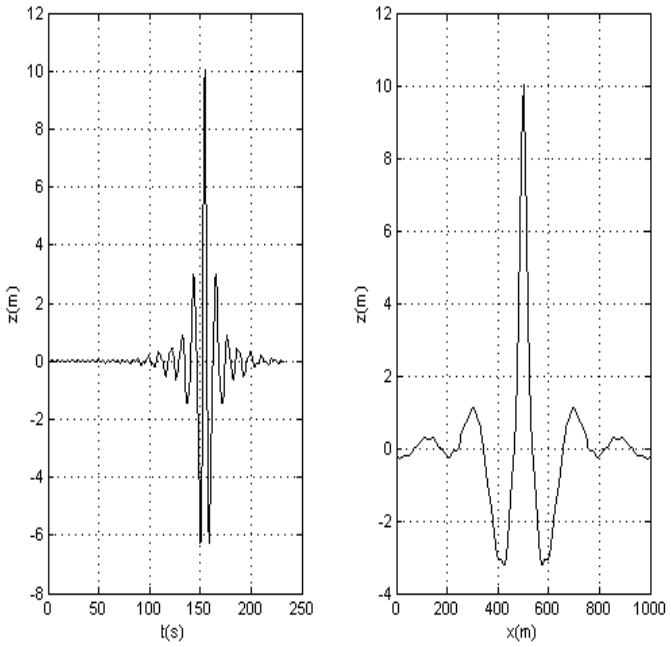

Figure 12: Plots of the theoretical wave, both temporal (left) and spatial (right)

In first instance, the highest wave (and thus the position of the GBS) was positioned at x = 500 (the theoretical wave maker is located at x = 0), leading to a corresponding Ts (the time at which the wave will reach that position) of 154 s. This distance between the focus point and the numerical wave maker suggests a computational domain that is large both in spatial and in temporal sense. This will lead to long simulation times. However, some gains can be made. Reflection should be avoided as much as possible. As we see in the figure above, the first 'relevant' wave occurs at t = 99 s. This means that the reflection of this wave must not return to the position of the GBS within 55 s. Given a wave phase speed of approximately 13 m/s the minimal distance between the GBS and a numerical wave maker in the simulation should not be less than 350 m. Further, beside the fact that Ts is smaller if a shorter domain is chosen, it is possible to start at some $t_1 > 0$; it is sufficient to prescribe the water height and the velocity field at t_1 provided these values are not too large at that time.

Keeping the aspects mentioned above in mind, the applicability of the linear theory for our purposes was investigated. Three situations, with increasing difficulty, were investigated:

- Deep water, low waves
- Deep water, high waves
- Shallow water, high waves

The first situation, with a water depth of 100 m and a wave height of 5.1 m (measured in the temporal sense, as in the rest of this paper) performs numerically rather well. As can be seen in the first picture of Figure 13, the comparison between theory and numerical practice after 500 m (and the same order of grid cells), at the focus point is good. Given a vertical cell height of (in this case) 1 m, the numerical model seems to propagate the waves well.

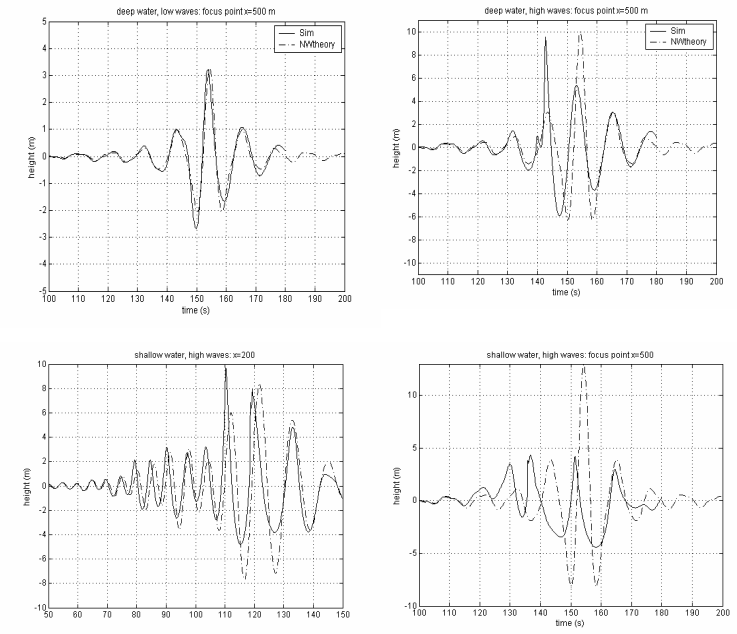

Figure 13: Propagation of the newWave. Upper left picture: Water height in focus point with deep water and low waves. Upper right picture: focus point; deep water, high waves. Second row: shallow water and high waves; water height at x=200m (left) and at the focus point (right).

If we keep the water depth constant and increase the wave height to 16 m, the non-linear dispersion effect begins to play a role. The steepening is more than in theory. Due to this effect the highest wave comes too early, and the theoretically highest wave has already overturned when it reaches the focus point. This wave is consequently much lower (see the upper right picture of Figure 13).

In the last situation, with a water depth decreased to 30 m, early steepening and breaking caused the waves at the desired focus point to be far too low. This can be seen in the second row of Figure 13. At x = 200m (left-hand picture)) significant steepening already occurs: the wave before the theoretically highest wave becomes actually the largest one. At x = 500 (right-hand picture), no correspondence between the theory and the simulation can be observed anymore. Note that this problem of early breaking waves has also been observed in the basin tests.

So the generated high linear NewWaves cannot be sustained in shallow water. It should be noted that previous simulations with regular 5th order Stokes waves performed better. This point needs further investigation. For the present study, the following pragmatic approach was chosen.

The GBS was put closer to the wave maker, before the theoretical focus point. As observed, the steepening begins well before the focus point. This enables us to pick appropriate points, before the focus point (x = 500 m) but after the slope (x = 350 m) with the desired wave height (after some trial and errors). In this way we were able to reach most of the required wave heights except the highest.

Numerical results: the jet

Simulations were performed with the specified waves and the effect of the run-up was studied. Due to the wave direction, the simulations could be done in a 2D domain, thus allowing a fine grid (although 3D simulations were also performed, see Figure 14) .

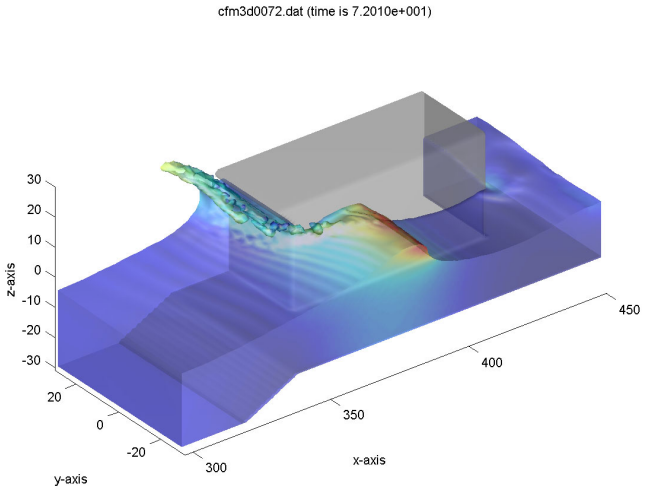

Figure 14: snapshot of a 3D simulation of the wave run-up

Figure 15 shows some simulation results with a box type GBS. The time between two consecutive snapshots is about 1.1 s.

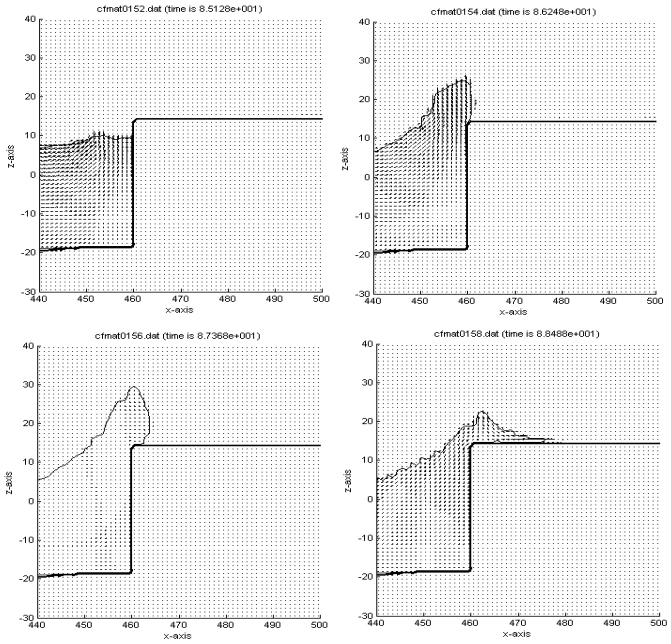

Figure 15: A low jet develops in front of the GBS

As seen in the model tests, the simulations showed that a run up jet was created in front of the GBS. A typical evolution of the rising and falling of a jet is shown in the figure:

- Wave reflection in front of the GBS (upper left figure)
- Development of water jet in front of the GBS with high vertical velocity (upper right figure)
- Jet at maximum height, velocities are reduced to zero, starting to fall down on the deck (lower left figure)
- Water jet impinging on the deck, resulting in high pressures on the deck and large horizontal velocities (lower right figure).

As was observed in the model tests, simulations with a wave deflector on top of the side of the GBS show that a deflector is very effective to diverge the jet away from the GBS. In Figure 16, four snapshots are shown. The time between two consecutive snapshots is one second.

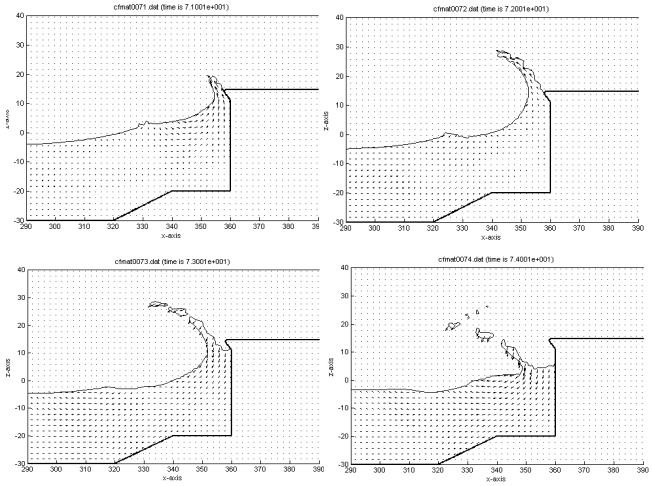

Figure 16: the jet is redirected by the deflector

- First, the jet starts to develop. Due to the deflector, it is immediately redirected to the left, away from the GBS.
- The jet approaches its maximum height, already 20m back from the GBS.
- The jet breaks up and falls down again.
- Further breaking up and dispersion of the jet.

Numerical results: contribution of wind

To study the contribution of the wind, it was decided to implement wind forces in ComFLOW. However, the method does not model the air, only the fluid (one-phase flow). Therefore, the following method was chosen:

- Wind is modelled as an external force on exposed fluid particles.
- This external force only acts at the surface (of a wave or a jet), like the atmospheric pressure, but it is unidirectional. More specific, this force will only act on the wind side of the jet and will have a horizontal direction.
- The wind velocity can be taken as the following vertical profile (Figure 17):

$$V(z) = V_{10}\left(\frac{z}{10}\right)^{0.14}$$

- The pressure is taken as the stagnatic pressure according to

$$P = \frac{1}{2}\rho V^2$$

with ρ being the density of air, V the wind velocity and A the projected area in vertical direction.

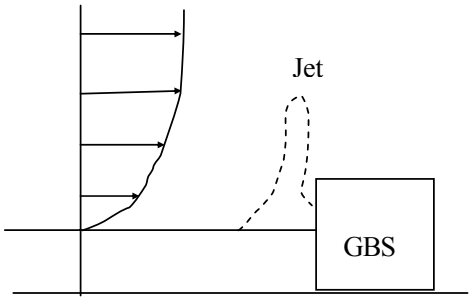

Figure 17: Schematic impression of the wind force

As an example, the effect of the wind on a water column in rest was studied. The wind speed was very high: V = 200 m/s. Snapshots are shown in Figure 18. In each subfigure, five contours are drawn, at respectively t = 0 s, t = 0.6 s, t = 1.2 s, t = 1.8 s and t = 2.4 s. The water column in the first sub picture has a thickness of 5 m, the column in the right-hand sub picture measures 10 m. With the thin jet more water comes on the deck.

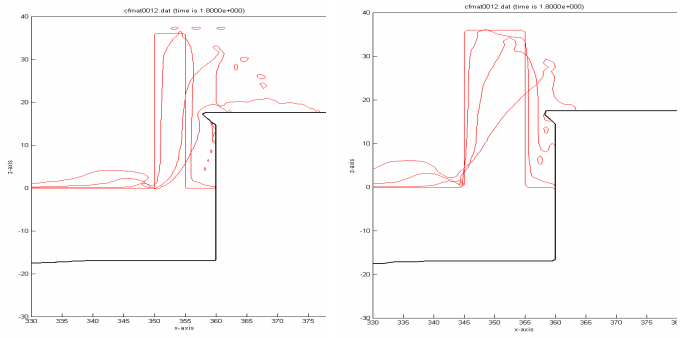

5 m **10 m**

Figure 18: Effect of a strong wind on a static water column with a width of 5 m and 10 m

The expectation was that the strong wind (the wind speed was set at 41 m/s) could possible redirect the jet in the direction of, and over, the deck. As can be seen at the combined snapshots (Figure 19) the effect is rather moderate (the dotted line represents the surface in a simulation without wind). This limited effect is mainly caused by the short time in which the jet actually exists, the thickness of the jet and the effectivity of the deflector in redirecting the jet. Note that the wind pressure on the surface is equivalent to 1 kPa: still considerable, but not excessive.

After these simulations, we did two additional runs (wind and no wind) but *without* the deflector. Here the wind indeed influences the amount of water on the deck; see Figure 20: Impact of a high jet without wind (left) and with wind (right) . The time between two consecutive snapshots is one second. The left–hand figures show the jet without wind, the right-hand figures the jet with wind included. Although this difference does not seem large, the amount of water on the deck is quite larger in the latter case. This can also be seen in Figure 21 showing time series of the vertical force on the deck.

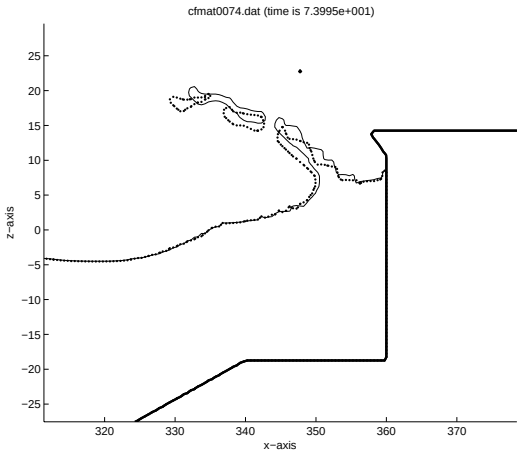

Figure 19: The effect of wind on the shape of the jet. Dotted line: without wind; continuous line: with wind

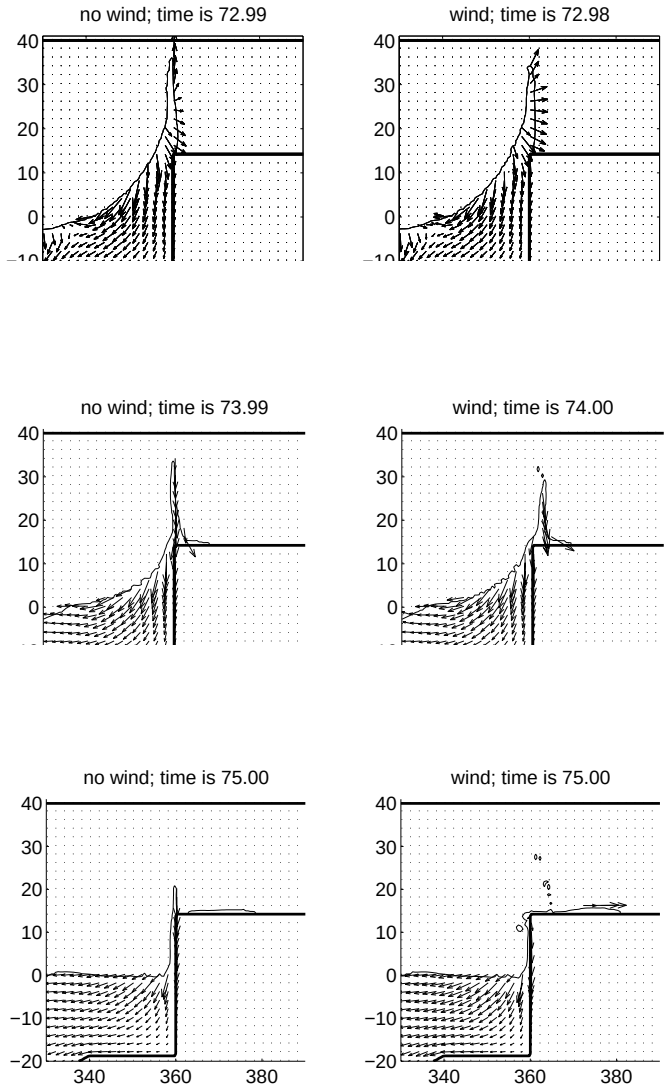

Figure 20: Impact of a high jet without wind (left) and with wind (right)

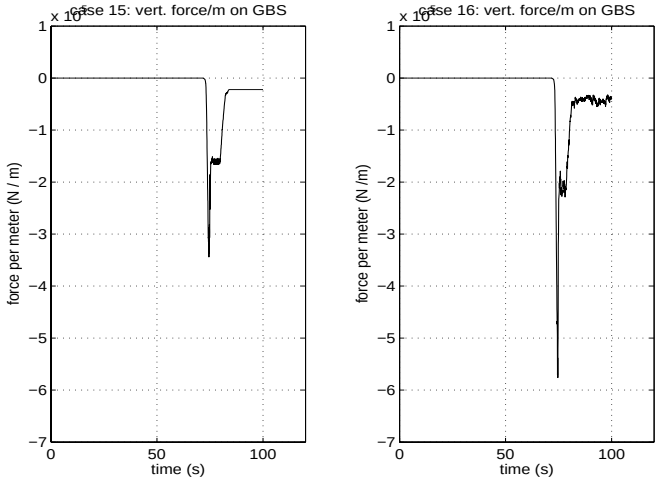

Figure 21: Total vertical force on the deck of the GBS. Left picture: without wind; right picture: with wind.

CONCLUSIONS

These preliminary investigations gave useful insight in the run up of waves close to a GBS. The agreement of the deflected jet between the basin tests and the numerical simulations is visually obvious. However, thorough validation has yet to be done. The most important observations concerning the numerical simulations are:

- The use of the NewWave in shallow water is limited due to its linearity.
- The deflector effectively redirects the jets away from the GBS
- The wind has hardly any effect but can increase the water load on the deck in the case of vertical jets.

In the near future, the numerical code will be extended in the following aspects:

- Improve the numerical wave maker to study the effect of real wave groups as part of irregular sea states.
- Improve the free surface description.
- Include the modelling of the air (two-phase flow).

ACKNOWLEDGEMENT

Shell International Exploration and Production is acknowledged for the permission to present the results in this paper. The discussions about the method and results with George Forristall and other members of the Shell team were very stimulating.

REFERENCES

1. Buchner, B.; "Green Water on Ship-type Offshore Structures", PhD thesis Delft University of Technology, 2002.

2. Buchner, B., Bunnik, T.H.J., Fekken, G. and Veldman, A.E.P.; "A Numerical Study on Wave Run Up on an FPSO Bow", OMAE2001, Rio de Janeiro, 2001.

3. Buchner, B., van Dijk A.W.V. and de Wilde, J.J. (2001), "Numerical multiple-body simulations of side-by-side mooring to an FPSO", ISOPE, Stavanger, 2001.

4. Buchner, B, Bunnik, T, Honig, D and Meskers, G, "A New Simulation Method for the Installation of Subsea Structures from the Splash Zone to the Ultra Deep", DOT conference, November 19-21, 2003.

5. Buchner, B., Loots. G.E., Forristal, G.Z and Iperen, E.J. van;"Hydrodynamics aspects of gravity based structures in shallow water", Offshore Technology Conference, Houston, May 2004.

6. Daalen, E.F.G. van, Kleefsman, K.M.T., Gerrits, J., Luth, H.R. and Veldman, A.E.P.; "Anti Roll Tank Simulations with a Volume Of Fluid (VOF) based Navier-Stokes Solver", 23rd Symposium on Naval Hydrodynamics, Val de Reuil, September 2000.

7. Fekken, G., Veldman, A.E.P. and Buchner, B.; "Simulation of Green Water Flow Using the Navier-Stokes Equations", Seventh International Conference on Numerical Ship Hydromechanics, Nantes, 1999.

8. Gerrits, J., Loots, G.E., Fekken, G. and Veldman, A.E.P.; "Liquid Sloshing on Earth and in Space", In: Moving Boundaries V (Sarler, B., Brebbia, C.A. and Power, H. Eds.) WIT Press, Southampton, pp 111-120, 1999.

9. Gerrits, J.; "Dynamics of Liquid-Filled Spacecraft", Numerical Simulation of Coupled Solid-Liquid Dynamics, PhD thesis, RuG, 2001.

10. Hirt, C.W. and Nichols, B.D.; "Volume Of Fluid (VOF) Method for the Dynamics of Free Boundaries", Journal of Computational Physics, 39, pp 201-225, 1981.

11. Kleefsman, K.M.T., Fekken, G., Veldman, A.E.P., Bunnik, T., Buchner, B. and Iwanowski, B.; "Prediction of green water and wave impact loading using a Navier-Stokes Based Simulation Tool", OMAE conference, Oslo, 2002.

12. Tromans P.S., Anaturk, A.R. and Hagemeijer P., "A new model for the kinematics of large ocean waves", ISOPE, Edinburgh, 1991.